

Scaling in Electroweak Reactions: What Is It Useful for?

J.A. Caballero

Dpto. Física Atómica, Molecular y Nuclear, Universidad de Sevilla, 41080
Sevilla, Spain

Abstract. Scaling clearly emerges from the analysis of world (e, e') data, hence it constitutes a strong constraint for any theoretical model trying to describe lepton-nucleus scattering. In past years we have investigated extensively this phenomenon showing how a model based on the Relativistic Impulse Approximation (RIA) is capable of reproducing not only scaling but also the specific shape of the experimental scaling function. However, a basic question still remains: why scaling is so important and what is it useful for? In this work I discuss how scaling can be used to make predictions on some basic properties in Nuclear Physics, such as nucleon momentum distributions, spectral functions and the Coulomb Sum Rule.

1 Introduction

The phenomenon of y -scaling emerges from the analysis of quasielastic (QE) (e, e') reactions. The scaling function, defined as the QE (e, e') differential cross section divided by the single-nucleon cross section is shown to depend only on a single variable, y , given as a particular combination of the two independent variables in the process, namely the energy and momentum transfers, ω and q . In the QE domain the basic mechanism in (e, e') reactions on nuclei corresponds to elastic scattering from individual nucleons in the nuclear medium. This implies that the inclusive (e, e') cross section is mainly constructed from the exclusive $(e, e'N)$ process, including the contribution of all nucleons in the target and integrating over all (unobserved) ejected nucleon variables. This approach constitutes the basis of the Impulse Approximation (IA).

The IA provides an intuitive explanation on how the scaling behavior emerges from the analysis of data. In the Plane Wave Impulse Approximation (PWIA) the $(e, e'N)$ differential cross section factorizes in two basic terms: the electron-nucleon cross section (σ^{eN}) for a moving, off-shell nucleon and the spectral function that gives the combined probability to find a nucleon of certain momentum and energy in the nucleus [1–3]. Assuming the spectral function to be isospin independent, and σ^{eN} to have a very mild dependence on the missing momentum and excitation energy, the inclusive QE (e, e') cross section is writ-

Scaling in Electroweak Reactions

ten in the form

$$\left[\frac{d\sigma}{d\epsilon' d\Omega'} \right]_{(e,e')} \cong \bar{\sigma}^e(q, \omega; p = |y|, \mathcal{E} = 0) \cdot F(q, \omega), \quad (1)$$

where the single-nucleon cross section is evaluated at the special kinematics $p = |y|$ and $\mathcal{E} = 0$ (the residual nucleus in its ground state).

The function $F(q, \omega)$ in Eq. (1) is known as the scaling function and it is given in PWIA in terms of the spectral function:

$$F(q, \omega) = 2\pi \iint_{\Sigma(q, \omega)} p dp d\mathcal{E} S(p, \mathcal{E}). \quad (2)$$

It is important to point out that only in the case in which it would be possible to extend the kinematically allowed region $\Sigma(q, \omega)$ to infinity in the excitation energy plane, *i.e.*, $\mathcal{E}_{max} \rightarrow \infty$, would the scaling function be directly linked to the true momentum distribution of the A -nuclear system: $n(p) \equiv \int_0^\infty d\mathcal{E} S(p, \mathcal{E})$. However, guided by the PWIA result in Eq. (1), an experimental scaling function can be also defined by dividing the experimental QE (e, e') cross section by the single-nucleon function, $\bar{\sigma}^e$. At high enough values of the momentum transfer q , the function $F_{exp}(q, \omega)$ has been shown to satisfy scaling in the region below the QE peak, that is, F_{exp} becomes only a function of the scaling variable y (see [4–7] for details).

Furthermore, based on the analysis performed with the Relativistic Fermi Gas (RFG) model, and making use of the separate longitudinal (L) and transverse (T) (e, e') data, experimental superscaling functions have been introduced:

$$f_{exp}(q, \omega) \equiv k_F F_{exp}(q, \omega) \quad (3)$$

$$f_{exp}^{L(T)}(q, \omega) \equiv k_F F_{exp}^{L(T)}(q, \omega), \quad (4)$$

where k_F is the Fermi momentum. In particular, the L response has been shown to superscale, *i.e.*, f_{exp}^L shows only a very mild dependence upon the momentum transfer q (first-kind scaling) and the nuclear system considered (second-kind scaling). This has led to introduce a universal experimental superscaling function that constitutes a strong constraint for any theoretical model describing QE electron scattering. Not only should the superscaling behavior be fulfilled, but also the specific shape of f_{exp}^L must be reproduced.

The scaling properties of the longitudinal data provide also an alternative procedure to get some insight into the Coulomb Sum Rule (CSR). Indeed, enormous experimental efforts have been made at different laboratories, Saclay [8–10], Bates [11], JLAB [12], to get separated longitudinal and transverse contributions from QE electron scattering data. The analysis of data and its impact on the CSR for different nuclei have been discussed in the literature, leading to different conclusions. Jourdan concluded that the integrated longitudinal (L) response function saturates for q high enough at the 100% of the CSR limit [13].

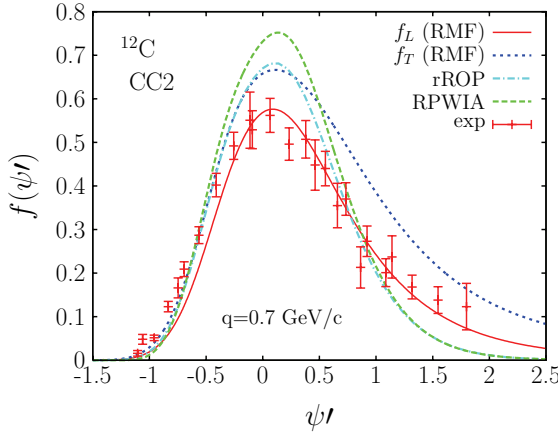


Figure 1. Superscaling function for $^{12}C(e, e')$ evaluated with the RPWIA, rROP and RMF approaches compared to the experimental function.

On the contrary, from Saclay data [8] Morgenstern and Meziani concluded the existence of a significant quenching of the CSR [10].

The experimental superscaling function has an asymmetric shape, with a long tail exhibiting strength for energy transfers well beyond the RFG domain. The presence of this tail is of relevance for the CSR analysis, as the sum rule requires integration of the strength in the whole energy transfer range (up to infinity), which is of course not feasible from the experimental point of view.

In recent works [14–16] it has been shown that the Relativistic Mean Field (RMF) model reproduces satisfactorily the magnitude and detailed shape of f_L^{exp} . This is clearly illustrated in Figure 1 where we present the superscaling function evaluated for different descriptions of FSI: real part of the relativistic optical potential (rROP), plane wave limit (RPWIA) and presence of the scalar and vector terms in the relativistic mean field potential (RMF). A comparison with the experimental L superscaling function is provided, showing that the RMF approach follows closely the behaviour of data describing also the asymmetrical shape of f_L^{exp} .

2 Nucleon Momentum Distribution and the Scaling Function

In this section we revisit the “usual” procedure to obtain the nucleon momentum distribution function from the analysis of QE (e, e') data (for more details see [17]). The usual procedure considered in previous work [18] has been based on the expression:

$$n(k) = \left[\frac{-1}{2\pi y} \left(\frac{\partial F}{\partial y} \right) \right]_{|y|=k}, \quad (5)$$

Scaling in Electroweak Reactions

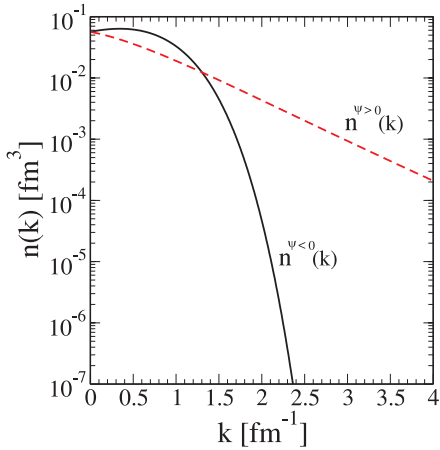


Figure 2. Nucleon momentum distribution extracted through the derivative of the super-scaling function given by the Gumbel probability density.

which has been widely applied in the negative- y region. In what follows we extend this study to the positive- y region based on the universal superscaling function introduced from the analysis of the separated longitudinal data. We may write

$$n(k) = -\frac{1}{2\pi k} \frac{1}{k_F} \left[\frac{df(\psi)}{d(k_F|\psi|)} \right]_{k_F|\psi|=k}. \quad (6)$$

Note that if the superscaling function is not symmetric with respect to ψ , as is the case for the experimental data, the above expression yields different momentum distributions for negative and positive values of ψ , which will be denoted by $n^<$ and $n^>$, respectively.

The results corresponding to the Gumbel distribution (see Ref. [17]) are presented in Figure 2. As expected, $n^{\psi<0}$ and $n^{\psi>0}$ coincide in the limiting case $k = 0$. For missing momenta up to $k \sim 1 \text{ fm}^{-1}$ the main contribution resides in $n^<$. At $k \simeq 1.3 - 1.4 \text{ fm}^{-1}$, *i.e.*, k close to the Fermi momentum, $n^<$ and $n^>$ cross each other, with $n^>$ being much higher for larger k -values. In fact, whereas $n^<$ shows a steep slope when k increases, which is in accordance with results based on independent-particle model descriptions, $n^>$ presents a high momentum tail very far from $n^<$ and hence from shell-model results. The presence of the tail at high momentum values in the nucleon momentum distribution is a clear signature of the importance of nucleon-nucleon correlations. Since the spectral function maps very different regions in the $(\mathcal{E} - k)$ plane for negative and positive y , the joint analysis of the two kinematical regions can provide important clues in the knowledge of NN correlations.

For completeness, $n^<(k)$ and $n^>(k)$ obtained from Gumbel distribution (solid lines) are compared with the RFG prediction (n_{RFG}), the shell-model re-

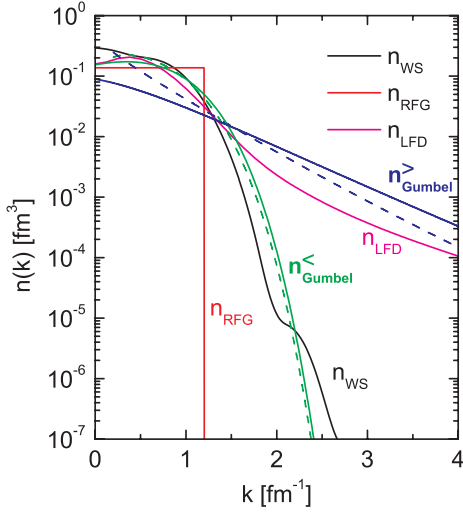


Figure 3. The nucleon momentum distribution extracted from the scaling function. For comparison are given the momentum distributions from the Relativistic Fermi Gas model (n_{RFG}), from the shell model (n_{WS}) and from the Light Front Dynamics (n_{LFD}).

sults (n_{WS}), as well as n_{LFD} obtained within the Light-Front Dynamics (LFD) approach [19, 20].

3 The Coulomb Sum Rule

The explicit expression for the CSR, widely used by experimentalists in the analysis of the separate L -data [8, 11], is written as

$$CSR(q) = \frac{1}{Z} \int_{\omega^+}^{\infty} \frac{R^L(q, \omega)}{\tilde{G}_E^2(Q^2)} d\omega \quad (7)$$

with the effective electric form factor given by

$$\tilde{G}_E^2(Q^2) = \left[G_{Ep}^2(Q^2) + \frac{N}{Z} G_{En}^2(Q^2) \right] \frac{(1+\tau)}{(1+2\tau)}, \quad (8)$$

where N and Z are the neutron and proton numbers of the target, respectively, and G_{Ep} and G_{En} the Sachs electric form factors for proton and neutron. The term τ is the usual dimensionless quantity, $\tau \equiv |Q^2|/4M_N^2$ with M_N the nucleon mass. The lower limit in the integration ω^+ includes all inelastic contributions but excludes the elastic peak.

An analog of the CSR can be also introduced in terms of the superscaled function and the scaling variable by taking into account the explicit expression

Scaling in Electroweak Reactions

of the longitudinal superscaling function,

$$CSR_{scal}(q) = \int_{-\infty}^{\infty} d\psi' f_L(\psi') . \quad (9)$$

Expression (7) used by experimentalists does not exactly correspond to Eq. (9) due to the fully relativistic expressions involved in the longitudinal scaling function [7] and to the different integration variable. Thus, in order to set down the impact of the particular CSR expression on the analysis of data, in what follows we compare results corresponding to Eqs. (7) and (9). The analysis is presented in Figure 4 for three nuclei: ^{12}C (top panel), ^{40}Ca (middle) and ^{56}Fe (bottom). In each case we show how the CSR behaves as a function of the energy transfer ω for three different values of the momentum transfer q : 0.3, 0.5 and 0.7 GeV/c. We compare the results corresponding to Eq. (7), denoted as CSR (dashed line), with the ones evaluated through the scaling function (9), denoted as Scaling (solid line). We observe that both expressions for the CSR lead to similar results, hence drawing analogous conclusions. All results in Figure 4 have been obtained with the RMF model.

Comparing the results obtained for the three nuclei, the CSR dependence

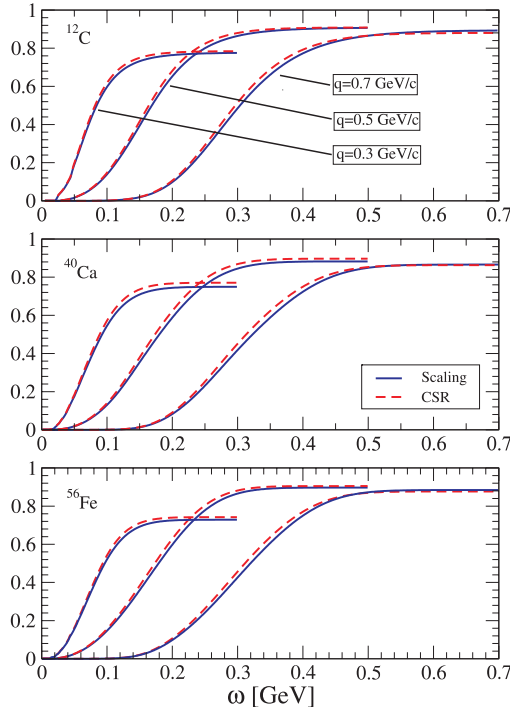


Figure 4. Coulomb sum rule as a function of the energy transfer. Results obtained using the expression of the CSR given by Eq. (7) are compared with predictions based on the scaling analysis (9).

with the target is seen to be very tiny. The CSR saturates to almost the same value for the three nuclei: ~ 0.9 for $q = 0.5$ and 0.7 GeV/c and ~ 0.7 for $q = 0.3$ GeV/c. Moreover, the behavior of the CSR is similar for the three targets, getting saturation, at each q -value, for very close transferred energies.

Comparison between CSR theoretical results and experimental data requires to extract the Coulomb sum rule from the longitudinal response data by performing the integrals in Eqs. (7), (9) using as upper integration limits the specific ω -cutoff values employed by the experimentalists. In particular, in the case of ^{40}Ca , different experiments, Bates [11] and Saclay [8], have considered different ω_{max} -values as integration limits.

In Figure 5 we present results for ^{40}Ca corresponding to RMF (top panel) and RPWIA (bottom) approaches. The CSR is shown as a function of the scaling variable $\psi'(q, \omega)$. For each q we also plot the value of the scaling variable ψ' corresponding to the specific ω -cutoffs given in the experimental papers. These regions are presented as shadowed areas, where the color indicates the specific q -value which is directly connected with the corresponding (same color) theoretical CSR result.

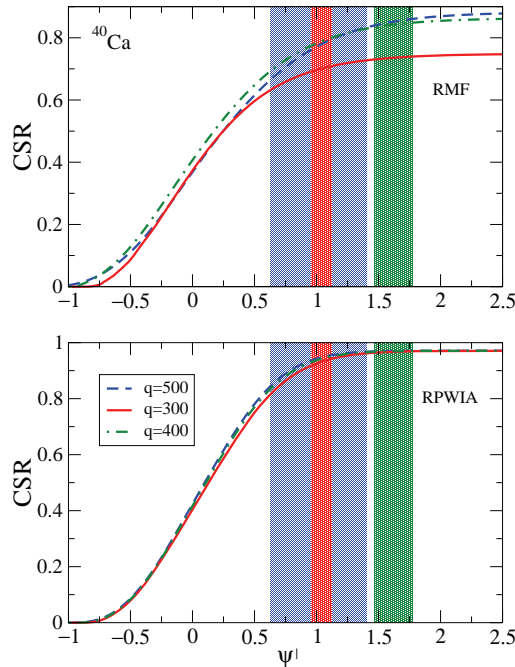


Figure 5. Coulomb sum rule as a function of the scaling variable ψ' for ^{40}Ca . Top panel refers to results obtained within the RMF approach and bottom to RPWIA. The shadowed bands refer to the energy transfer cutoffs considered in the experiments. Each color refers to a different q -value (see labels). Lower limits in each band correspond to Bates values and higher ones to Saclay integration cutoff.

Scaling in Electroweak Reactions

Results in Figure 5 illustrate clearly the amount of saturation reached by the CSR at the maximum ω -loss taken from the experiment. In the particular case of $q = 500$ MeV/c the wide blue shadowed area is linked to the very different ω -cutoffs considered at Bates and Saclay, $\omega_{max} = 220$ MeV and 290 MeV, respectively. For Saclay experiment [8], *i.e.*, upper limit in the shadowed band, the CSR model evaluated up to the experimental cutoff includes $\sim 95\%$ ($\sim 100\%$) contribution of the total CSR strength in the RMF (RPWIA) approach. On the contrary, the contribution (integrated up to ω_{max}) reduces to $\sim 75\%$ ($\sim 95\%$) for RMF (RPWIA) in the case of the maximum energy loss used at Bates [11] (lower limit of the band, $\omega_{max} = 220$ MeV).

To conclude, a comparison between theory and experimental data is provided in Figure 6. First, in the left-top panel theoretical results for the CSR evaluated with the RMF approach applied to ^{40}Ca (red circles) and ^{12}C (green triangles) are presented. In both cases, CSR has been obtained extending the upper integration limit to the maximum value permitted by the kinematics. On the contrary, in the right-top panel of Figure 6 we compare Bates CSR data with

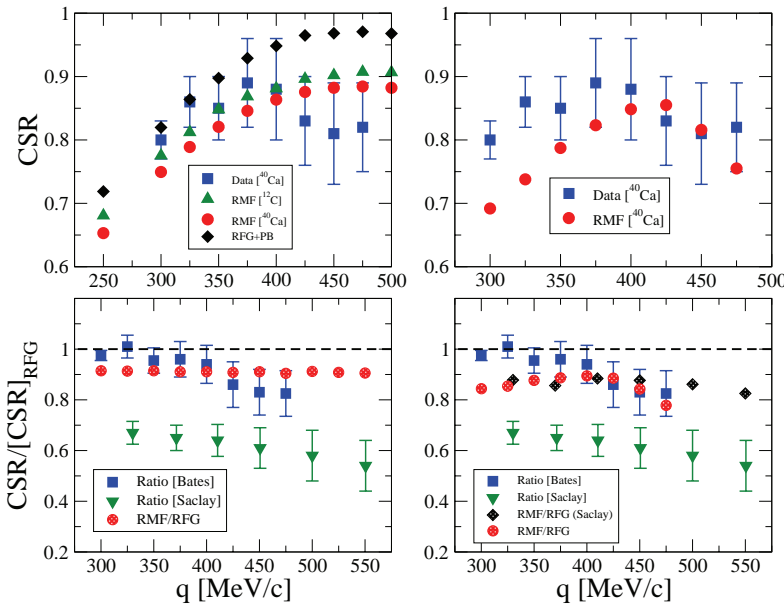


Figure 6. Coulomb sum rule compared to data. Top-left panel shows results obtained with the RMF for ^{12}C (green triangles) and ^{40}Ca (red circles) and RFG with Pauli blocking (black diamonds). In all cases, integration in Eq. (9) has been extended to the whole region allowed by kinematics. Theoretical results are compared with data from Bates corresponding to ^{40}Ca . Top-right panel: as in previous case but RMF calculations evaluated using the ω -cutoff values given in [11]. Bottom panels present the ratio between RMF results and RFG ones compared to data from Bates and Saclay.

RMF theoretical results, but these now evaluated using as upper integration limits the same ω_{max} values considered in the experiment. From these results, we conclude that the Coulomb sum rule from RMF reaches $\sim 85 - 95\%$ of its saturated value if truncation at the experimental ω -cutoff is taken. The comparison with CSR results obtained from data measured at Bates for ^{40}Ca has shown its accordance with the RMF approach. These results show that no further quenching is needed to describe the longitudinal response measured at BATES. This is in contrast with data measured at Saclay showing a reduction of the L channel of the order of $\sim 30 - 40\%$ [8–10], in spite of the fact that in these experiments the cutoff in the energy transfer is larger than for Bates experiments. This can be clearly observed in the ratios shown in the bottom panels (for more details see Ref. [21]).

4 Conclusion

In the present work a study of the scaling function and its connection with the momentum distribution is presented. A close relationship between the two quantities exists using the PWIA and under some conditions for the kinematically allowed region. The “usual” analyses performed in the past to the region below the QE peak is extended here to the region above the peak, since the superscaling function is defined for both negative and positive values of the scaling variable. The considerations in the present work lead to results that are quite different from those obtained solely in the negative- y scaling region and give information about the energy and momentum distribution in the spectral function.

The “universal” superscaling function extracted from the analysis of separated longitudinal data for QE (e, e') scattering, has been applied to the study of the Coulomb Sum Rule. In order to compare our theoretical predictions with experiment, we have analyzed the role played by the cutoff ω -value considered as upper integration limit in the expression of the CSR. From our results, we conclude that the Coulomb sum rule from RMF reaches $\sim 85 - 95\%$ of its saturated value if truncation at the experimental ω -cutoff is taken. The largest strength lost in CSR occurs for $q = 475$ MeV/c, and is of the order of $\sim 15\%$. The comparison with CSR results obtained from data measured at Bates for ^{40}Ca has shown its accordance with the RMF approach. These results show that no further quenching is needed to describe the longitudinal response measured at BATES, that shows a depletion of the free value of the order of $\sim 10 - 20\%$. This is in contrast with data measured at Saclay showing a reduction of the L channel of the order of $\sim 30 - 40\%$ [8–10]. The reasons for this difference would hopefully be clarified by the recent experiment at JLAB [12].

Acknowledgements

This work was partially supported by DGI (MICINN-Spain) contract FIS2008-04189, PCI2006-A7-0548, the Spanish Consolider-Ingenio programme CPAN

Scaling in Electroweak Reactions

(CSD2007-00042), by the Junta de Andalucía, and by the INFN-CICYT collaboration agreements INFN08-20 & FPA2008-03770-E/INFN. This work has been done in collaboration with A.N. Antonov, M.B. Barbaro, T.W. Donnelly, J.L. Herráez, M.V. Ivanov, M.C. Martínez and J.M. Udías.

References

- [1] S. Frullani and J. Mougey, *Adv. Nucl. Phys.* **14** (1984) 1.
- [2] S. Boffi, C. Giusti, F.D. Pacati, M. Radici, *Phys. Rep.* **226** (1993) 1; *Electromagnetic Response of Atomic Nuclei*, Oxford University Press, Oxford (1996).
- [3] J.J. Kelly, *Adv. Nucl. Phys.* **23** (1996) 75.
- [4] D. B. Day, J. S. McCarthy, T. W. Donnelly and I. Sick, *Ann. Rev. Nucl. Part. Sci.* **40** (1990) 357.
- [5] T.W. Donnelly and I. Sick, *Phys. Rev. Lett.* **82** (1999) 3212.
- [6] T.W. Donnelly and I. Sick, *Phys. Rev. C* **60** (1999) 065502.
- [7] C. Maieron, T.W. Donnelly and I. Sick, *Phys. Rev. C* **65** (2002) 025502.
- [8] Z.E. Meziani *et al.*, *Phys. Rev. Lett.* **52** (1984) 2130.
- [9] Z.E. Meziani *et al.*, *Phys. Rev. Lett.* **69** (1992) 41.
- [10] J. Morgenstern, Z.E. Meziani, *Phys. Lett. B* **515** (2001) 269.
- [11] C.F. Williamson *et al.*, *Phys. Rev. C* **56** (1997) 3152.
- [12] Jian-Ping Chen, Seonho Choi, Zein-Eddine Meziani, spokesperson, JLAB E-05-110, hallaweb.jlab.org/experiment/E05-110/exp_home. Precision Measurement of Longitudinal and Transverse Response Functions of Quasi-Elastic Scattering in the Momentum Transfer Range $0.55 \text{ GeV}/c < q < 0.9 \text{ GeV}/c$
- [13] J. Jourdan, *Nucl. Phys. A* **603** (1996) 117.
- [14] J.A. Caballero, J.E. Amaro, M.B. Barbaro, T.W. Donnelly, C. Maieron and J.M. Udías, *Phys. Rev. Lett.* **95** (2005) 252502.
- [15] J.A. Caballero, *Phys. Rev. C* **74** (2006) 054603.
- [16] J.E. Amaro, M.B. Barbaro, J.A. Caballero, T.W. Donnelly, J.M. Udías, *Phys. Rev. C* **75** (2007) 034613.
- [17] J.A. Caballero, M.B. Barbaro, A.N. Antonov, M.V. Ivanov, T.W. Donnelly, *Phys. Rev. C* **81** (2010) 055502.
- [18] C. Ciofi degli Atti, E. Pace, G. Salmé, *Phys. Rev. C* **39** (1989) 259; *ibid* **C43** (1991) 1155.
- [19] A.N. Antonov, M.K. Gaidarov, M.V. Ivanov, D.N. Kadrev, G.Z. Krumova, P.E. Hodgson, H.V. von Geramb, *Phys. Rev. C* **65** (2002) 024306.
- [20] A.N. Antonov, M.V. Ivanov, M.K. Gaidarov, E. Moya de Guerra, J.A. Caballero, M.B. Barbaro, J.M. Udias, and P. Sarriuguren, *Phys. Rev. C* **74** (2006) 054603.
- [21] J.A. Caballero, M.C. Martínez, J.L. Herráez, J.M. Udfas, *Phys. Lett. B* **688** (2010) 250.